P2.13 MICROPHYSICAL SIZE SORTING REVEALED BY DUAL-POLARIZATION DOPPLER RADAR

MATTHEW R. KUMJIAN AND ALEXANDER V. RYZHKOV

CIMMS/OU/NSSL, Norman, Oklahoma

1. INTRODUCTION

The trajectories of hydrometeors in precipitating storms are dependent on the airflow patterns within such storms. Because the terminal velocity of raindrops increases with the drop diameter, drops will be advected throughout the storm at varying rates. The consequence of this is a separation or sorting of the drops based on their size. In convective storms, such size sorting can result in areas with significantly altered drop size distributions (DSDs). With the advent of dual-polarization radars, measurements at orthogonal polarizations allow estimating median drop sizes and thus observing DSD characteristics. Such observations can be used to infer the locations of ongoing size sorting in the storm.

This study examines several kinematic mechanisms of size sorting that occur in many convective thunderstorms. The next section presents the basic principles of size sorting. The following sections discuss several size sorting mechanisms, analyzing them through polarimetric radar observations of convective storms and simple numerical models. The size sorting mechanisms discussed in this paper include differential sedimentation, updrafts, strong rotation, and vertical veering wind shear. The latter mechanism results in a low-level signature in differential reflectivity (Z_{DR}) known as the Z_{DR} arc, which is given its own discussion (Section 7). Through a simple explicit microphysics numerical model we show that the magnitude of the Z_{DR} arc is proportional to the storm-relative environmental helicity (SREH) and that it is a possible indicator of storm severity and potential for tornadogenesis. With the anticipated polarimetric upgrade of the NEXRAD WSR-88D network in mind, the importance of identifying such microphysical processes is discussed.

Corresponding author address: Matthew Kumjian, CIMMS/NSSL, 120 David L. Boren Blvd., Norman, OK, 73072. Matthew.Kumjian@noaa.gov

2. SIZE SORTING PRINCIPLES

Gunn and Kinzer (1949) measured the terminal velocities of liquid water drops of varying size in the laboratory. They found that terminal fall speed of the drop increases monotonically with its diameter. Based on this data, numerous mathematical models for the relationship of v_t to D have been suggested, several of which are plotted in Figure 1. Atlas et al. (1973) presented a fairly accurate empirical equation:

$$v_t(D) = 9.65 - 10.3\exp(-0.6D) \quad (1)$$

where D is in mm. Equation (1) is valid for drops between 0.6 mm and 5.8 mm. For calculating the moments of the DSD, a power law fit is quite useful. Atlas and Ulbrich (1977) show that the relation

$$v_t(D) = 3.78D^{0.67} \quad (2)$$

fits the data for drops with diameters (D in mm) ranging from 0.5 mm to 5 mm. It is important to note that (1) and (2) are valid at sea level pressure, so correction factors should be utilized at higher altitudes (e.g., Foote and duToit 1969).

More recently Brandes et al. (2002) provide a polynomial function that better fits the Gunn and Kinzer (1949) data for most drop sizes (D in mm):

$$v_t(D) = -0.1021 + 4.932D - 0.9551D^2 + 0.07934D^3 - 0.002362D^4 \quad (3)$$

Since raindrops fall at different velocities, larger drops that fall faster will be exposed to airflow patterns in the storm for shorter durations than smaller drops. Consequently,

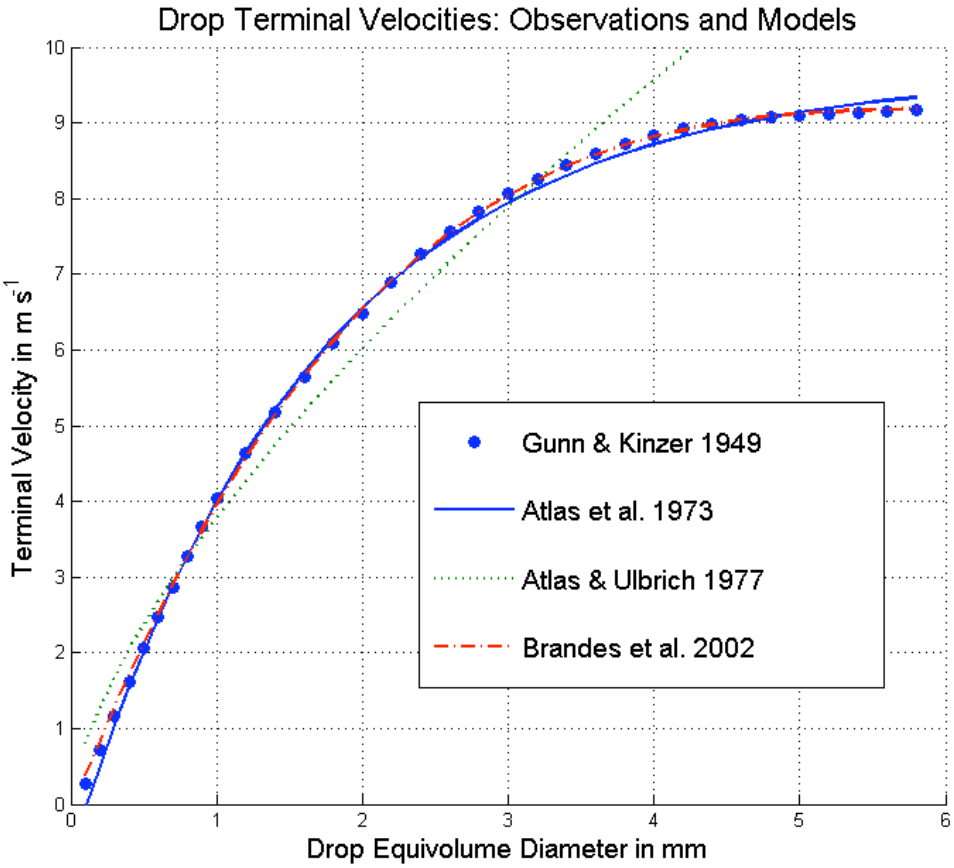

Fig. 1: The relationship between raindrop terminal velocities and drop equivolume diameter. The blue dots represent the Gunn and Kinzer (1949) experimental data. Three mathematical models of this data are shown: the Atlas et al. (1973) exponential relationship (solid blue line), the Atlas and Ulbrich (1977) power law relationship (dotted green line), and the Brandes et al. (2002) polynomial function (dash-dot red line).

smaller drops are advected further. The smallest drops follow the winds with little deviation. On the other hand, large drops typically fall against the prevailing wind patterns, resulting in shorter downstream trajectories. This separation of drop sizes due to a combination of air motions in storms and their different characteristic fall speeds is what we define as size sorting. In severe convective storms, size sorting can be quite vigorous, leading to particularly skewed DSDs.

Although essentially undetectable with single polarization radars, changes in the DSD throughout a storm will be observable using polarization diversity. This is because the oblateness of raindrops increases with diameter (Pruppacher and Pitter 1971). Since Z_{DR} (the ratio of backscattered power at orthogonal polarizations) is a measure of the oblateness of scatterers in the resolution volume (Seliga and Bringi 1976), inferences can be made about the median drop size of the hydrometeors being observed. Thus, when storm airflow patterns are such that vigorous size sorting of drops takes place, the resulting observed Z_{DR} field should exhibit signs of modified DSDs. For example, in locations where most small drops are advected away, the median drop size in those regions would be relatively large (compared to other parts of the storm), resulting in an increase in Z_{DR}. In this way a careful analysis of polarimetric radar data can garner information about the airflow within storms. The following sections discuss different mechanisms of size sorting observed in convective storms.

3. DIFFERENTIAL SEDIMENTATION

In the absence of any wind in a precipitating cloud, size sorting of drops can still occur. This is due to the difference in terminal fall speeds, as discussed in Section 1. If a cloud begins to precipitate, larger drops fall faster than smaller drops. So, before a steady-state is achieved, polarimetric observations would show an enhancement of Z_{DR} descending towards the ground as larger raindrops fall further than smaller drops. Differential sedimentation will occur for any spectrum of drop sizes, provided it is not a monodisperse distribution, which is unlikely to occur naturally.

In a simple one-dimensional numerical model, a Marshall-Palmer inverse exponential DSD with a 30 mm hr^{-1} rainfall rate is initialized for a cloud that begins to precipitate from a base 2 km above the ground. Drop sizes range from 0.05 mm to 7.95 mm, in 0.1 mm increments. Drops of each size bin (80 in all) are tracked as they fall from the cloud. The polynomial function (3) is used for terminal velocities. No drop interactions or other effects such as evaporation and coalescence are included. After 200 seconds (but before the drops begin to reach the ground), vertical profiles of polarimetric variables are calculated using scattering amplitudes provided by a T-matrix code. A sharp increase in Z_{DR} at the leading edge of the precipitation is evident (Figure 2). Additionally, a decrease in reflectivity factors at both horizontal and vertical polarizations (Z_H and Z_V) as well as in specific differential phase (K_{DP}) occurs, primarily due to the lower total concentration of raindrops.

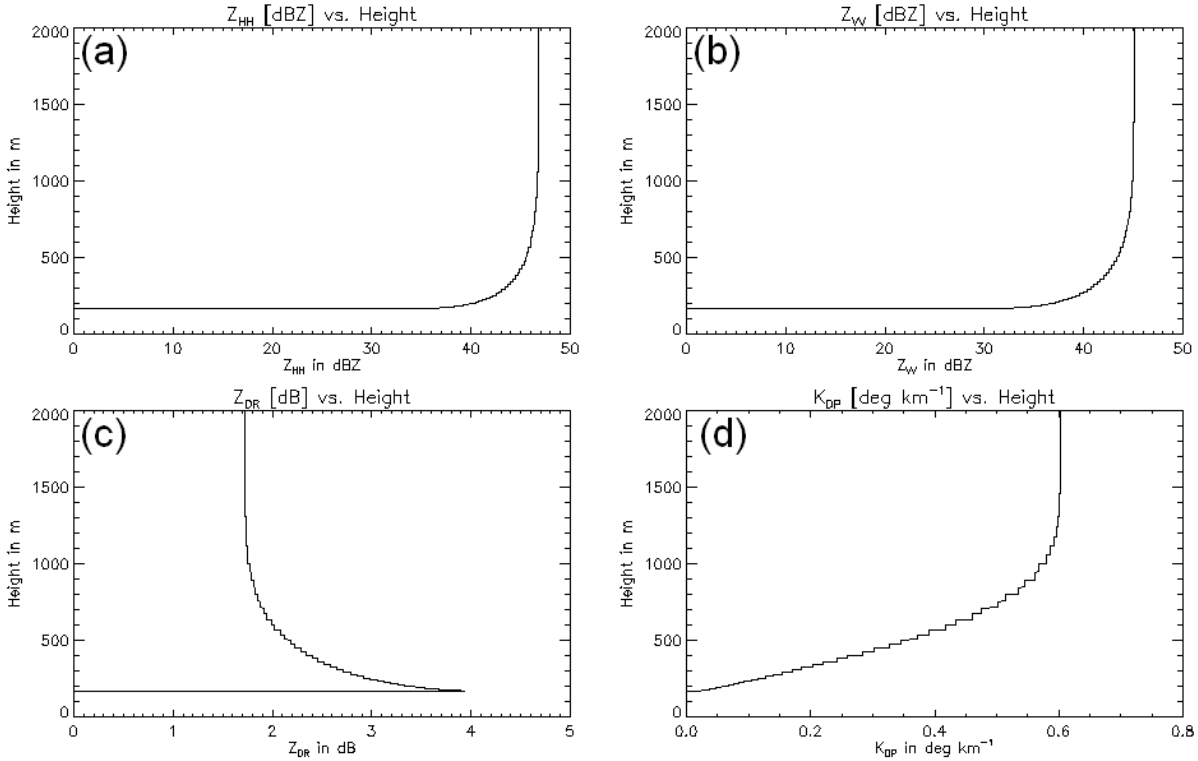

Fig. 2: Output from a model of a precipitating cloud (30 mm hr^{-1} rainfall rate) after t = 200 seconds. Vertical profiles of the following polarimetric variables are shown: (a) reflectivity factor at horizontal polarization (Z_H) in dBZ, (b) reflectivity factor at vertical polarization (Z_V) in dBZ, (c) differential reflectivity (Z_{DR}) in dB, (d) specific differential phase (K_{DP}) in deg km^{-1}.

4. UPDRAFTS: VERTICAL VELOCITIES

Vigorous size sorting occurs in convective storm updrafts since the vertical velocities typically exceed the terminal fall speeds of many smaller drops. In some cases (e.g., supercells) the updrafts are so intense that nearly all hydrometeors are lofted, resulting in a radar-observed weak echo region (WER) or bounded weak echo region (BWER) in Z_H. On the periphery of intense updrafts where upward vertical velocities are diminished, the larger drops are able to fall. Thus, columns of Z_{DR} are observed on the periphery of storm updrafts, extending from the ground to heights above the environmental melting layer[1]. In supercells, Z_{DR} columns are found on the inflow (right) flank of the updraft (Kumjian and Ryzhkov 2008).

5. ROTATION: CENTRIFUGING

Dowell et al. (2005) and Bluestein et al. (2007) show that violent rotation associated with tornadoes can produce ring-like structures in reflectivity factor Z_H (Fig. 4). The annular structures are produced when raindrops, hailstones, and nonmeteorological debris are centrifuged by the rotational motion. With single-polarization radar, these projectiles are indistinguishable and all contribute to the Z_H pattern. With dual-polarization radar, tornadic debris is marked by a distinct polarimetric tornadic debris signature (Ryzhkov et al. 2005), observed as anomalously low ρ_{HV}, near-zero Z_{DR}, and high Z_H (at S band). In contrast, hydrometeors are characterized by much higher ρ_{HV} values (generally > 0.90), with raindrops having intrinsic positive values of Z_{DR}.

In Figure 4, the polarimetric variables indicate different scatterers present in the tornado vortex. Within a 500 m radius of the center of the vortex (marked by a black dot), very low ρ_{HV} and Z_{DR} indicate nonmeteorological debris. Immediately surrounding this region is a band of higher Z_H, positive Z_{DR}, and high ρ_{HV}, all of which indicate liquid raindrops. Beyond this band, the far left portion of the domain shows reduced Z_H, very high Z_{DR}, and reduced ρ_{HV}. This indicates the presence of large drops or small, wet hailstones and a relative lack of smaller drops. This makes sense physically: the larger hydrometeors with larger terminal fall velocities are centrifuged further from the center of the vortex than smaller raindrops. The debris is usually large enough that it is centrifuged away from the vortex and falls rapidly to the ground. Thus, appreciable concentrations of large debris could be found near the center of the vortex at low levels, but are unlikely at higher levels. This is consistent with the hypothesis presented by single-polarization radar observational studies by Wurman et al. (1996) and Wurman and Gill (2000), and with the modeling done by Dowell et al. (2005), in which they proposed that the near-surface center ring of Z_H in the tornado is comprised of debris. It should be noted that the polarimetric TDS has been observed in the 8 May 2003 tornadic supercell reaching heights of over 2 km (e.g., Ryzhkov et al. 2005; Kumjian and Ryzhkov 2008). It is likely that the debris in this case was lighter (such as insulation), allowing the tornado to loft it to considerable heights without any appreciable centrifuging. Insulation from damaged and destroyed houses was in fact observed falling from the sky at substantial distances from the 8 May 2003 tornado (A. Schenkman, 2006, personal communication).

In contrast to tornadoes, mesocylcones are most likely too weak to cause observable centrifuging of raindrops. The vorticity of a strong mesocyclone in a supercell thunderstorm is typically a few orders of magnitude less than that of a tornado, because the mesocyclone length scales are much larger and the velocity scales are much smaller than tornadoes. Thus, appreciable centrifuging of raindrops is unlikely for mesocylcones. It is possible, however, that large hailstones may be centrifuged from particularly strong mesocyclones. Although probably not observable in Z_{DR} (since large hailstones tend to be quasi-spherical and thus characterized by intrinsic near-zero Z_{DR}), centrifuging of hailstones may be evident in the difference between Doppler velocity measurements at H and V polarizations

[1] Additionally, larger drops formed from melted ice particles that have fallen from the backsheared anvil could be recycled back into the updraft (e.g., Conway and Zrnic 1993).

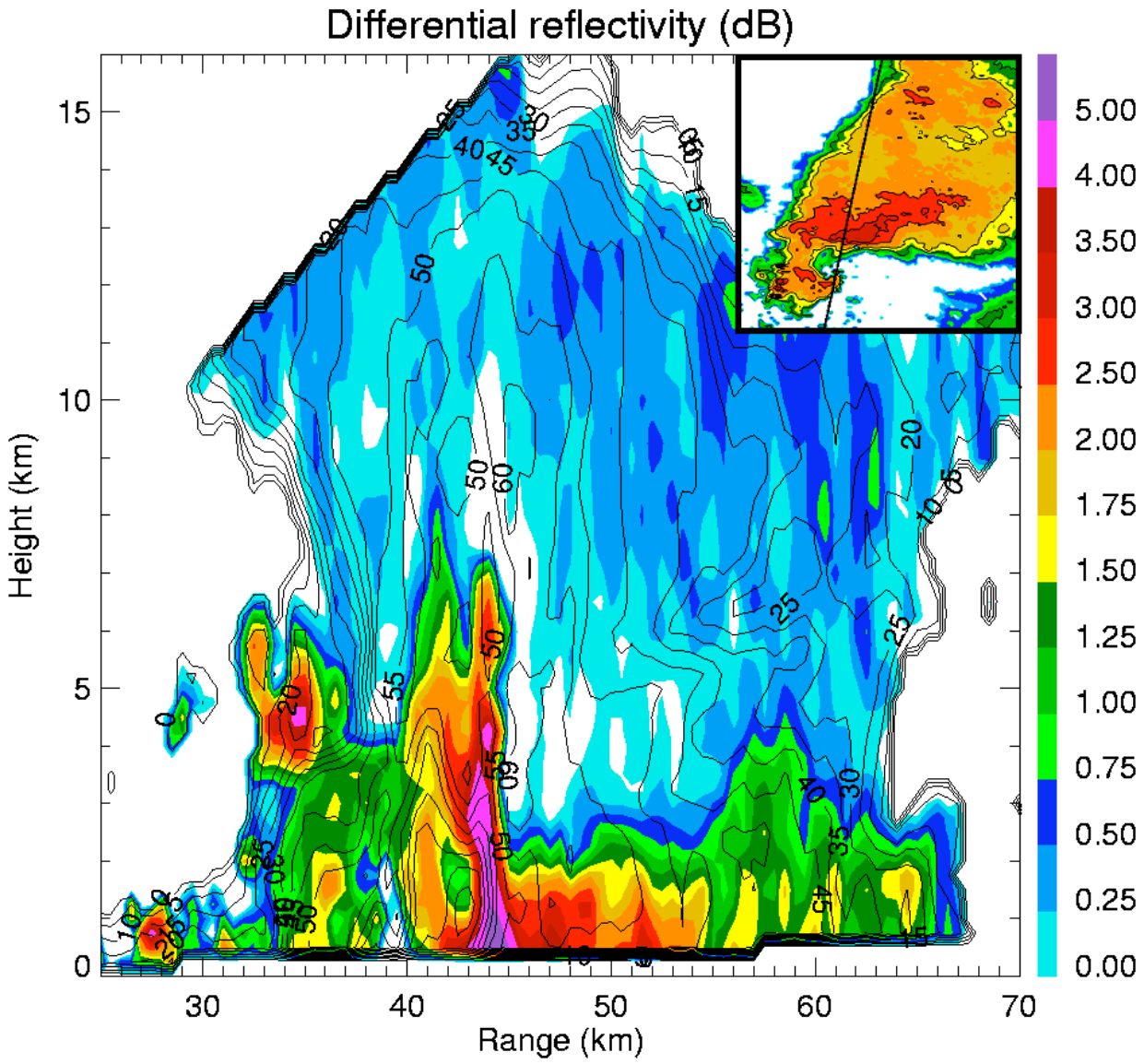

Fig. 3: An example Z_{DR} column from the 10 May 2003 tornadic supercell, shown in a vertical cross section. The column is centered at a range of about 44 km. The inset shows the lowest-level PPI of Z_H, the solid black line indicating where the cross section is taken. Adapted from Kumjian and Ryzhkov (2008).

within a resolution volume in the storm mesocyclone. However, this is beyond the scope of the present paper, which focuses on the size sorting of raindrops.

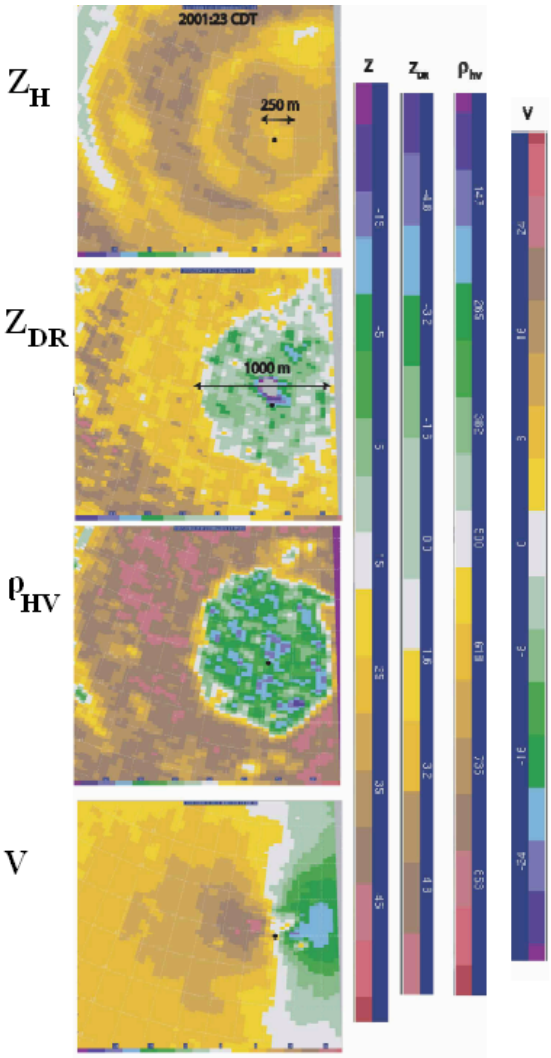

Fig. 4: Polarimetric observations of a tornado at X band. From top to bottom, the fields shown are Z_H (dBZ), Z_{DR} (dB), ρ_{HV}, and V (m s^{-1}). The scales are shown to the right of the panels. The center of the tornadic vortex is marked with a black dot in each panel. Adapted from Bluestein et al. 2007 (their Figure 4).

6. WIND SHEAR

a. Observations

Gunn and Marshall (1955) showed that wind shear causes size sorting of precipitation particles. Thus, strong wind shear in the environments of convective storms can cause significant size sorting in the falling precipitation. Strong horizontal flow differentially advects raindrops based on their size due to the size dependence of terminal velocities. Unidirectional wind shear coupled with updrafts along the leading edge of mesoscale convective systems result in a narrow region of very high Z_{DR} (> 3 dB) along the leading edge of such storms. This is routinely observed in squall lines with the polarimetric radar in Norman, OK (KOUN) and is visually observed as a sparse concentration of large drops as the squall line gust front passes overhead.

Winds that increase in speed and veer strongly with height are common in supercell environments (e.g., Fawbush and Miller 1954; Maddox 1976; Darkow and McCann 1977; Davies-Jones 1984). It is this strong veering wind shear that produces a signature intrinsic to supercell storms called the Z_{DR} arc (Kumjian and Ryzhkov 2007, 2008). This signature is observed as a narrow arc-shaped region of extremely high Z_{DR} on the Z_H gradient of the southern (inflow) edge of the forward-flank downdraft of supercells. Several examples from KOUN observations are shown in Figure 5.

The signature is a shallow one, typically only extending to a height of 1 – 2 km above the ground. This indicates that the strongest shear may be quite shallow near the surface. Further aloft in the storm, above the melting layer, the polarimetric variables indicate the presence of graupel downstream of the main updraft. Thus, it is graupel that falls and melts that produces the raindrops observed at the surface along the edge of the FFD. The low-level veering wind profile causes the smaller drops to be advected further into the FFD, whereas the largest drops fall “against” the flow. This results in a modified drop size distribution (DSD) along the southern edge of the FFD, one that consists of a sparse concentration of large drops. This modified DSD is frequently observed by storm spotters and storm intercept teams as they pass through this region of supercells. In the next section, we test this hypothesis of the origin of the Z_{DR} arc using a simple numerical model.

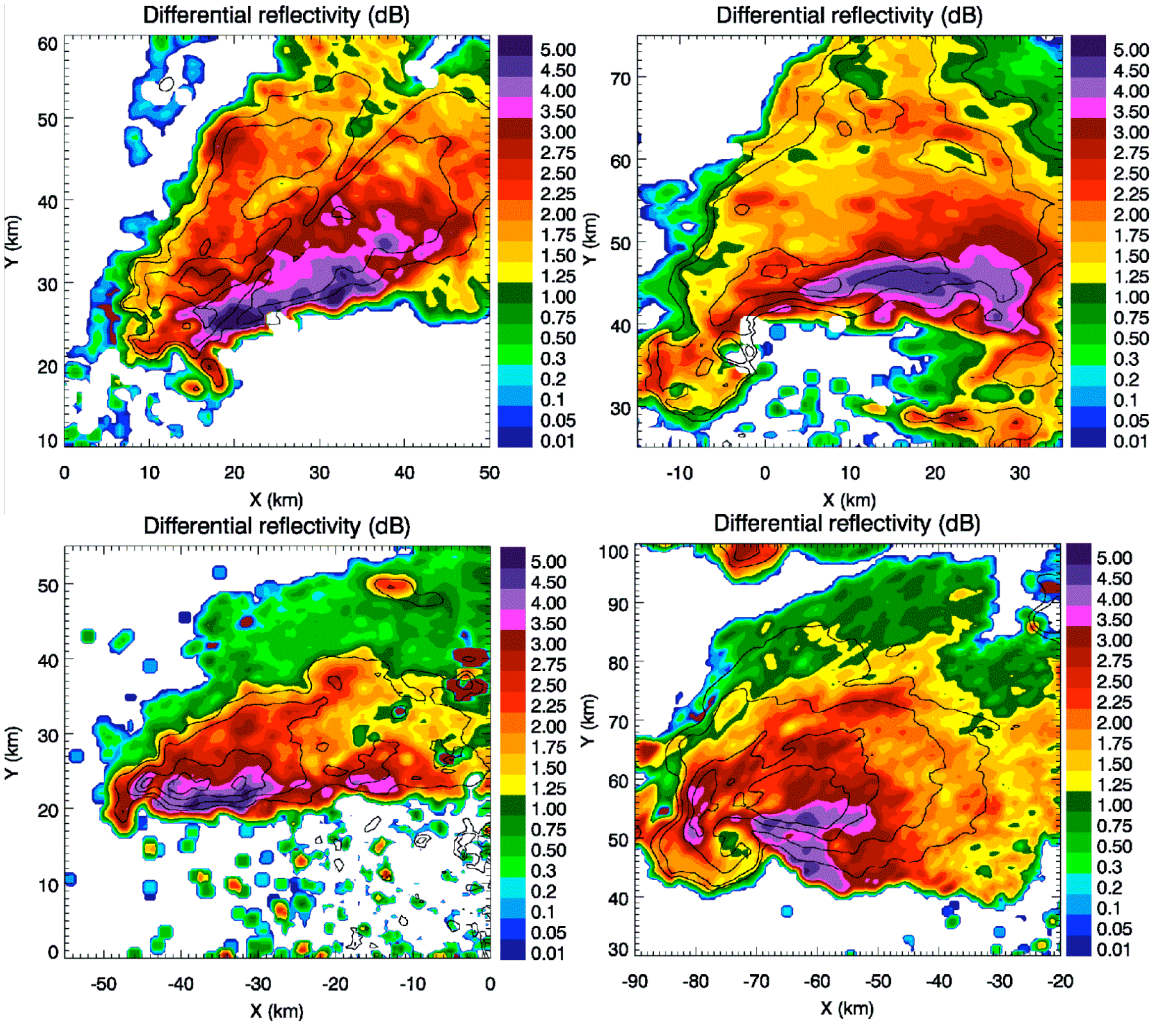

Fig. 5: Examples of Z_{DR} arcs from various storms: (a) 8 May 2003, 2234 UTC at 1.5°; (b) 10 May 2003, 0333 UTC at 0.5°; (c) 26 May 2004, 2346 UTC at 0.4°; (d) 30 May 2004, 0044 UTC at 0.5°. In each case, the arc is found along the gradient in Z_H on the southern edge (inflow side) of the forward flank downdraft (FFD).

b. The Model

To test the hypothesis, a simple model was constructed. At the top of the domain (3 km), a precipitating cloud is initiated at t = 0. The rainfall rate in the cloud is supposed to increase from 25 mm hr^{-1} at the periphery of the storm to 50 mm hr^{-1} at the center. The model is initialized with a Marshall-Palmer DSD, with a slope depending on the rainfall rate (no significant differences were found when other DSD models were used, including a Gamma distribution with the same initial Z_H, Z_{DR}, and K_{DP} pattern). There are eighty drop sizes (from 0.05 mm to 7.95 mm in 0.1 mm increments), and trajectories are calculated for each drop size. No drop interactions are considered. The drops fall according to a synthesis of the terminal velocity relationships in (1) and (2) through an environment with a prescribed wind profile, which is horizontally uniform throughout the domain. After allowing the drops to fall and advect for 3000 seconds, the polarimetric radar variables Z_H, Z_{DR}, and K_{DP} are calculated using the T-Matrix scattering amplitudes at selected altitudes. The results from several different vertical wind profiles are presented below.

c. The Results

To illustrate the model results from each of the wind profiles simulated in this analysis, the ensuing figures will show the polarimetric variables (Z_H, Z_{DR}, and K_{DP}) at three levels: 3.0 km, 1.5 km, and 0.4 km. As a

control run, the model is initiated with no wind; that is, the drops fall freely through the domain with zero horizontal motion. As expected, no Z_{DR} arc is observed since no size sorting occurs. The resulting polarimetric variables at 400 m are shown in Figure 6. The maximum value of Z_{DR} at 400 m (1.9 dB) is identical to the maximum value of the initial cloud.

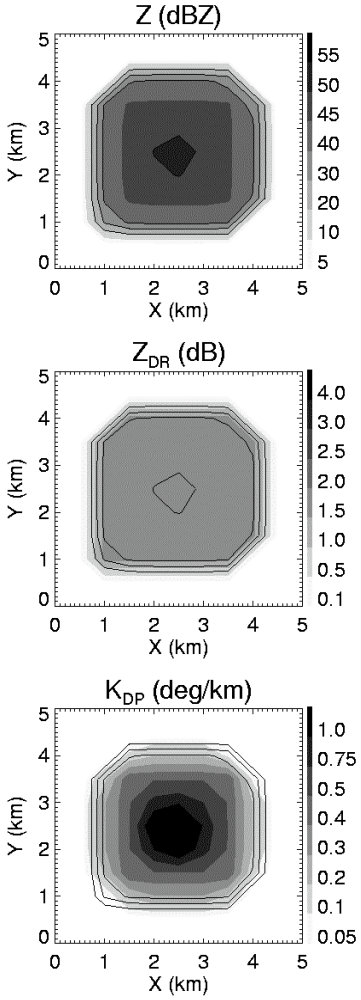

Fig. 6: Modeled polarimetric variables at 400 m after 3000 seconds for precipitation falling into an environment with no wind. From top to bottom, the fields shown are Z_H, Z_{DR}, and K_{DP}. The pattern of each of these variables is essentially the same as the initial cloud at 3 km (minor differences due to smoothing). Contours of Z_H are overlaid on each panel.

Next, we consider a veering wind profile. The environmental wind speed is constant at 10 m s^{-1}, but the wind direction veers from southerly at the surface to westerly at 3 km. The cloud itself is moving towards the east at 5 m s^{-1}, which results in storm-relative veering and speed shear, as seen in the hodograph in Figure 7.

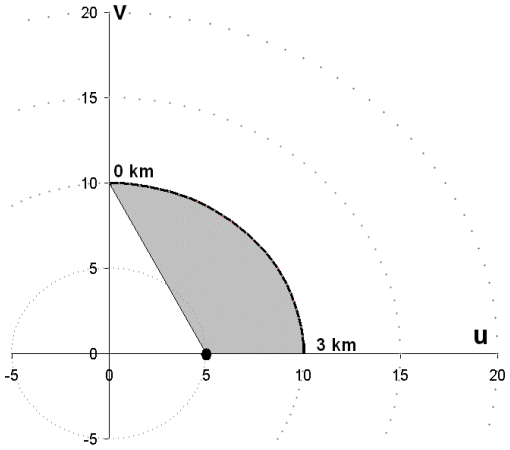

Fig. 7: Hodograph for experiment 1. The velocity components (u and v) are given in m s^{-1}. The black dot represents the storm motion vector, and the solid black line is the environmental hodograph, with the 0 km and 3 km altitude labeled. The size of the gray shaded area is proportional to the 0 – 3 km storm-relative environmental helicity (SREH).

The gray shaded area is proportional to the storm-relative environmental helicity (SREH; Davies-Jones 1984):

$$SREH = \int_0^{z'} \left(\vec{\mathbf{v}}_H - \vec{\mathbf{c}}\right) \cdot \nabla \times \vec{\mathbf{v}}_H \, dz \tag{4}$$

where $\vec{\mathbf{v}}_H$ is the horizontal velocity vector, $\vec{\mathbf{c}}$ is the storm motion vector, and *z*' is the top of the inflow layer, which is typically around 3 km (Davies-Jones 1984; Droegemeier et al. 1993; Markowski et al. 1999). The resulting fields of radar variables from this experiment are presented in Figure 8. Note that the fields have attained a steady state. It is clear that an enhancement of Z_{DR} along the southern edge of the storm is present at 1500 m, and it is even more prominent at 400 m. At 1500 m, the maximal Z_{DR} value is about 3.1 dB, whereas it is 3.6 dB at 400 m. The size and shape of the radar echo, as determined by the contours of Z_H, change as a function of height due to advection in the sheared environment. The maxima of Z_H and K_{DP} remain close to the center of the echo because these variables are mostly affected by total drop

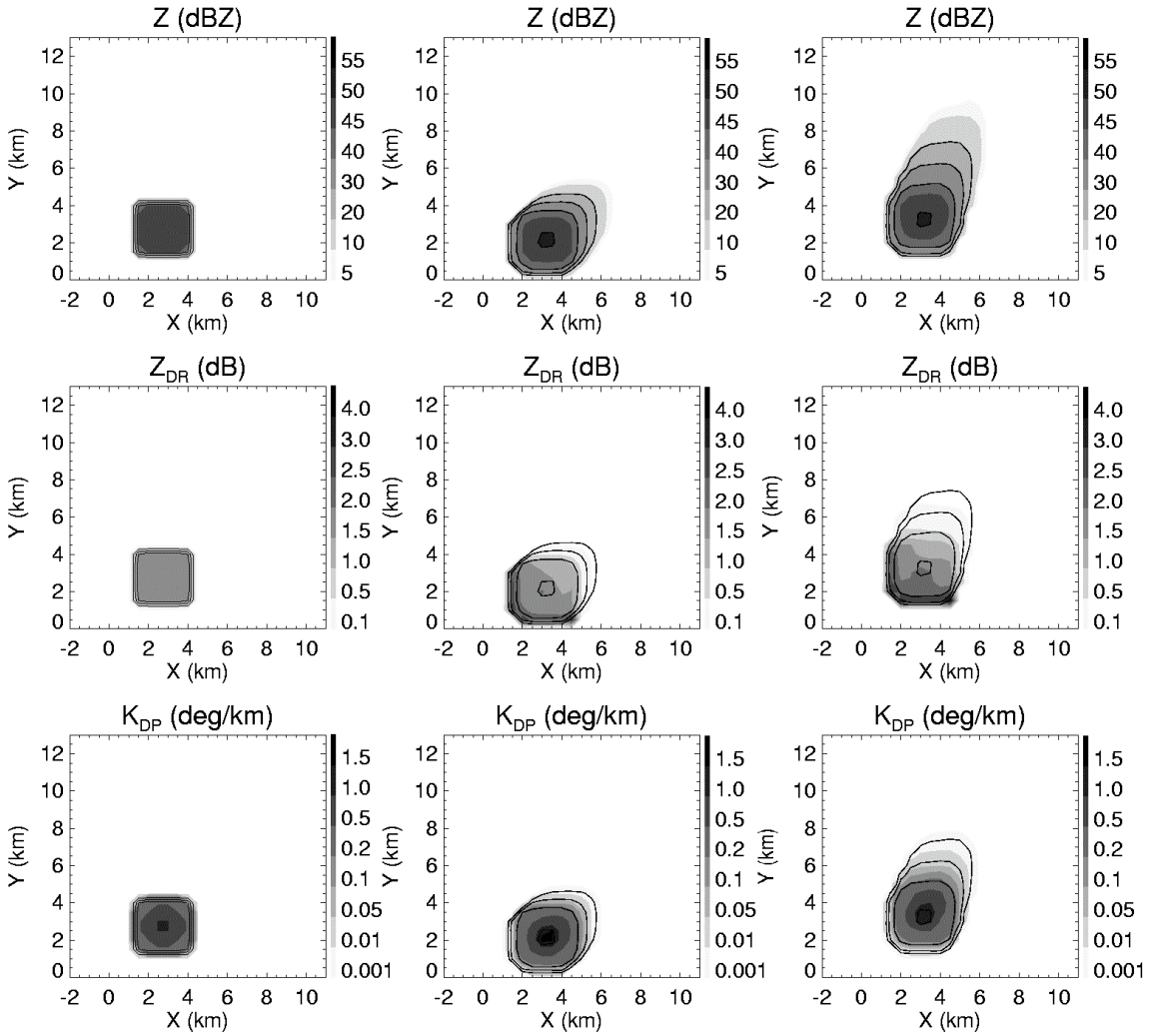

Fig. 8: Model results using the wind profile in Fig. 7. From left to right, the three polarimetric variable fields are shown for heights of 3.0 km, 1.5 km, and 0.4 km, respectively. The domain is relative to the variable fields and thus is not a particular fixed coordinate system. Contours of Z_H are overlaid on each panel.

concentration, whereas Z_{DR} is enhanced along the gradient in Z_H since Z_{DR} is not affected by concentration but by the mean diameter of the drops in the sampling volume.

Next, a similar wind profile is prescribed. This time, the environmental winds are stronger (15 m s^{-1}), and the storm motion is towards the east at 10 m s^{-1}, as shown in Figure 9. It is clear from a comparison between the hodographs in Fig. 7 and Fig. 9 that the SREH is greater in Figure 9. The resulting polarimetric variables are shown in Figure 10. Here we see that the enhancement of Z_{DR} along the southern edge of the storm is stronger, with maximal values at 400 m of 4.5 dB.

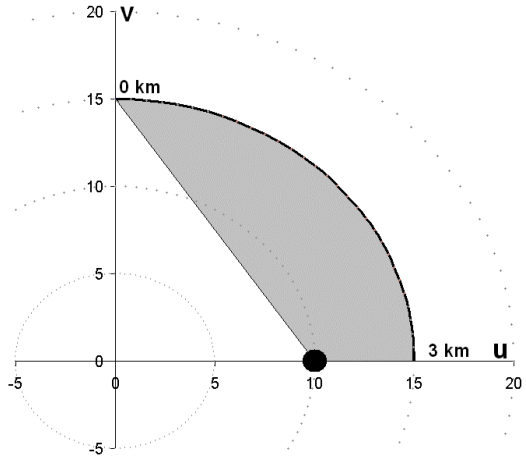

Fig. 9: Hodograph indicating the wind field used in experiment 2. The graphic scheme is the same as in Fig. 7.

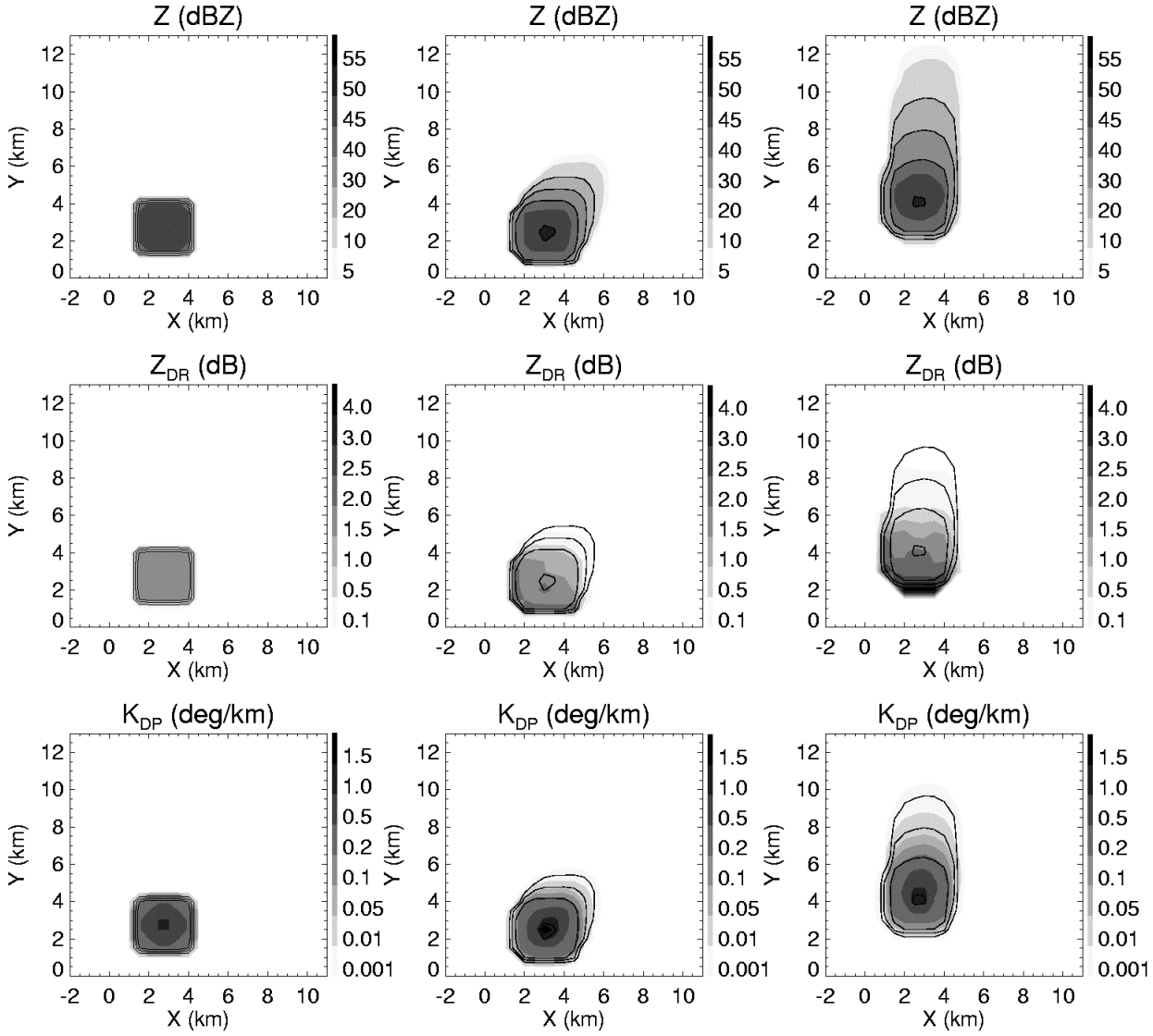

Fig. 10: As in Fig. 8, except for the hodograph in Fig. 9 (experiment 2).

To test the sensitivity of the results to the prescribed DSD model, we employ a gamma distribution (Ulbrich 1983) instead of the M-P:

$$N(D) = N_0 D^{\mu} \exp\left(-\Lambda_i D\right) \tag{5}$$

with the parameters N_0 = 4000 mm^{-1} m^{-3}, μ = 5.89, and Λ_1 = 3.6 mm^{-1}, Λ_2 = 3.7 mm^{-1}, and Λ_3 = 3.9 mm^{-1} (again, increasing rainfall rate towards the center of the cloud). This DSD gives a virtually identical initial profile of Z_H, Z_{DR}, and K_{DP}, and the resulting fields are very similar to Fig. 10, with the Z_{DR} along the southern edge of the storm attaining a maximum value of 4.4 dB at 400 m.

Instead of idealized wind profiles, we next model the 0 – 3 km sounding from the 9 May 2003 sounding at 00 UTC (for the 8 May tornadic supercell shown in Fig. 5). The hodograph is presented in Figure 11. Compared to the previous idealized hodographs, the general shape is similar (if the entire hodograph is rotated). However, the 9 May hodograph exhibits a shallow layer of very strong straight-line environmental shear near the surface (below 500 m), with strong veering immediately above. The storm motion for this case was determined by Esterheld and

Giuliano (2007, personal communication)[2]. The results from this model run are presented in Figure 12.

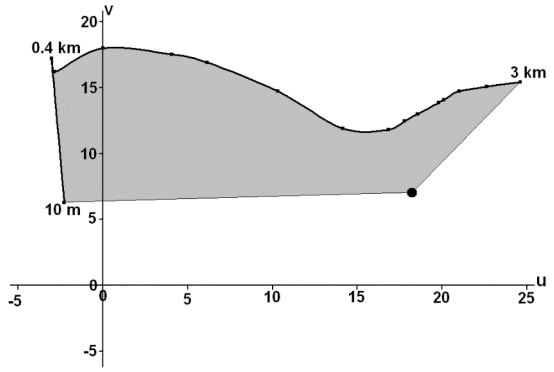

Fig. 11: As in Figs. 7, 9, but for the 9 May 2003 tornadic supercell 00 UTC sounding.

We see a very similar profile to the previous experiments at 1500 m and 400 m, with a strong Z_{DR} enhancement (4.5 dB) along the southern edge at 400 m. This value is quite close to the observed values in the Z_{DR} arc in the 8 May 2003 supercell. In fact, the alignment of the Z_{DR} arc is similar to the one observed (Figure 5).

7. DISCUSSION AND CONCLUSIONS

The Z_{DR} arc signature presented in the previous section is the manifestation of veering wind shear that is characteristic of an environment conducive to severe convective storms, especially supercells. It is observed in nontornadic and tornadic supercells alike, in different climate regions, seasons, and at different radar wavelengths (Kumjian and Ryzhkov 2008). Because this signature is related to a wind profile conducive for supercells (or updraft rotation), it is possible that the strength of this feature may be related to the SREH. From numerous simulations with different hodographs, a scatterplot of the SREH values (calculated from the hodographs) versus the maximal value of Z_{DR} along the southern edge of the storm at 400 m can be constructed. The 0.4 – 3 km SREH is used since the ZDR was calculated at 400 m. In some of the hodographs (e.g., the 9 May 2003 sounding, Fig. 11) a large amount of the SREH is found below 400 m. Thus, using the 0 – 3 km SREH would be inconsistent with the analysis. Although not a linear relationship, it appears from Figure 13 as if there is a positive correlation between SREH and the strength of the Z_{DR} arc.

Thus, the Z_{DR} arc may be of operational merit as a tool for estimating the strength of the SREH at the location of the storm. Markowski et al. (1998) show that SREH can vary considerably in space and time within severe weather environments. Since soundings are taken at widely spread "point" locations, estimates of the SREH from soundings may not be accurate. SREH estimated from the Z_{DR} arc is valid *at the storm's location*, which is of considerable importance. In addition, nonsupercellular convective storms that display a Z_{DR} arc may be in an environment similar to those typical of supercells. In other words, the storm may be moving into a region of enhanced low-level SREH. Since SREH is a measure of the component of the environmental vorticity that is streamwise (Davies-Jones 1984) to the inflow, the storm may develop rotation and should be closely monitored for intensification. An example of such a case is given in Kumjian and Ryzhkov (2008).

The coming NEXRAD network upgrade to dual-polarization capabilities is undoubtedly a significant progressive step for operational and research meteorologists alike. This paper demonstrates yet another benefit of polarimetry: the ability to observe manifestations of airflow patterns within severe convective storms through microphysical size sorting. The locations of updrafts, newly falling precipitation, rotation, and strong shear are evident in enhancements of the observed polarimetric variables, all of which are important for diagnosing the behavior and evolution of convective storms.

[2] This was a seminar presentation given at the National Weather Center in Norman, OK in August 2007 titled "Revisiting the hodograph: A new examination of low-level shear between storm classes."

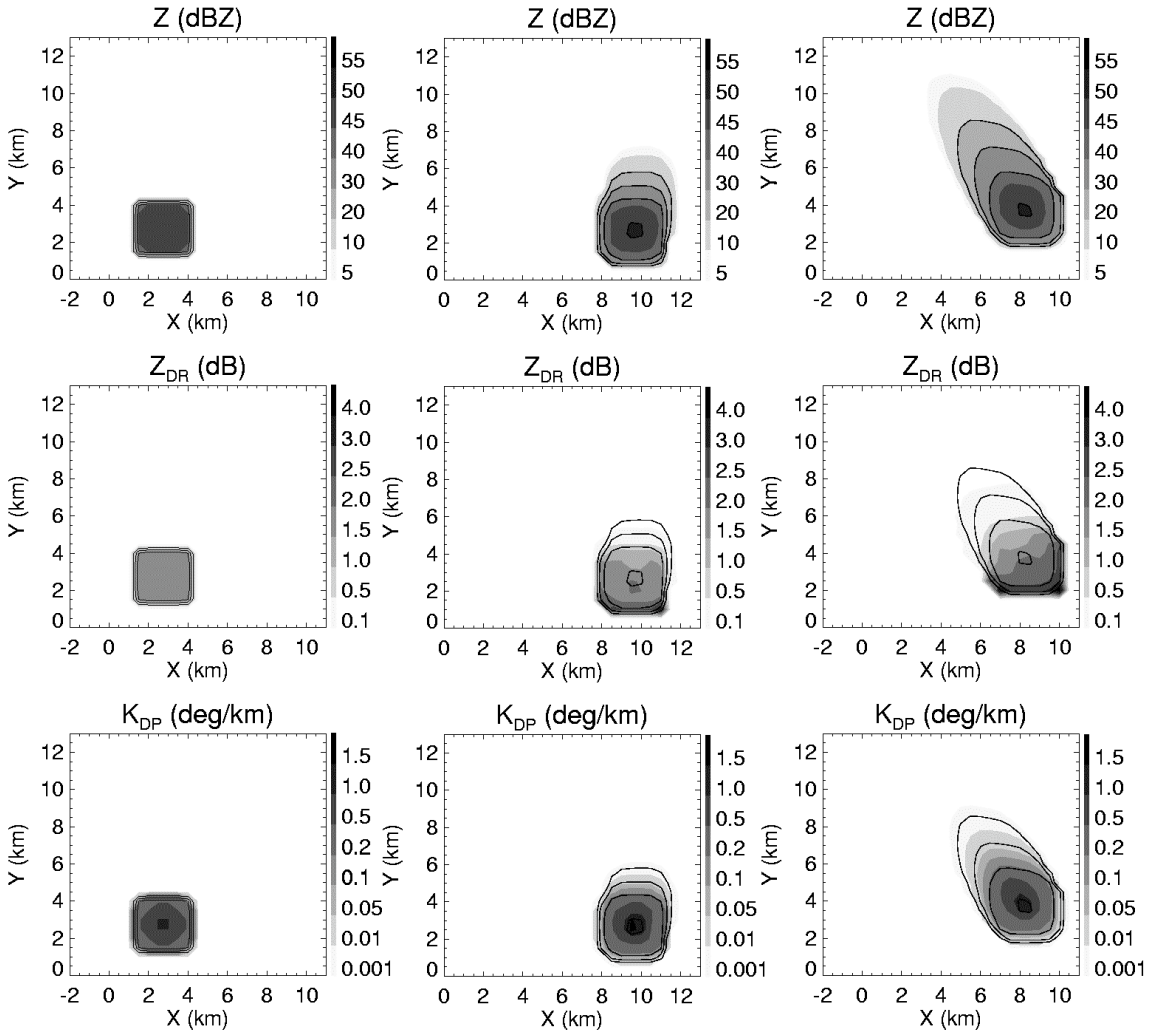

Fig. 12: As in Fig. 10, except for the 9 May 2003 hodograph shown in Fig. 11.

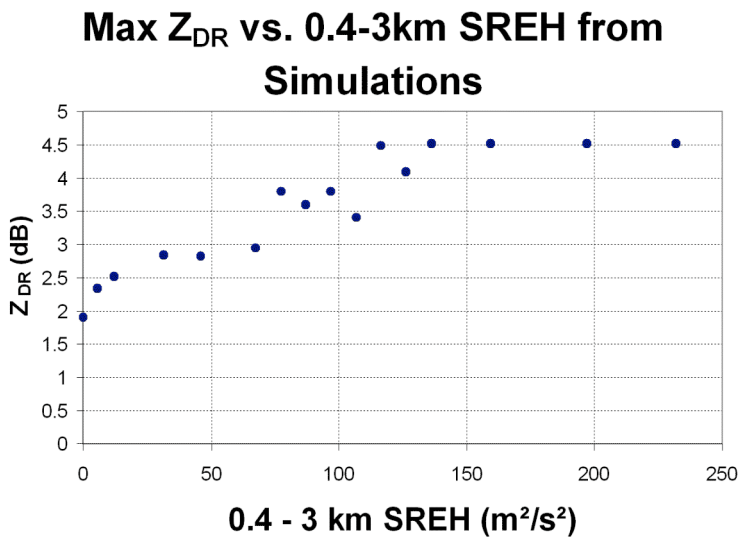

Fig. 13: Scatterplot of the maximal value of Z_{DR} along the southern edge of the modeled storm versus the SREH as computed from the experimental hodograph, based on several simulations.

8. ACKNOWLEDGEMENTS

This work evolved from part of a M.S. Thesis at the University of Oklahoma and is supported under the NSF grant ATM-0532107. Additional funding was provided by NOAA/Office of Oceanic and Atmospheric Research under NOAA-University of Oklahoma Cooperative Agreement #NA17RJ1227, U.S. Department of Commerce. We are grateful for public access to the University of Wyoming sounding archives.

9. REFERENCES

Atlas, D., R.C. Srivastava, and R.S. Sekhon, 1973: Doppler radar characteristics of precipitation at vertical incidence. *Rev. Geophys. Space Phys.*, **2**, 1-35.

Atlas, D. and C.W. Ulbrich, 1977: Path- and area-integrated rainfall measurement by microwave attenuation in the 1 – 3 cm band. *J. Appl. Meteor.*, **16**, 1322-1331.

Bluestein, H.B., M.M. French, R. L. Tanamachi, S. Frasier, K. Hardwick, F. Junyent, and A. Pazmany, 2007: Close-range observations of tornadoes in supercells made with a dual-polarization, X-band, mobile Doppler radar. *Mon. Wea. Rev.*, **135**, 1522-1543.

Brandes, E.A., G. Zhang, and J. Vivekanandan, 2002: Experiments in rainfall estimation with a polarimetric radar in a subtropical environment. *J. Appl. Meteor.*, **41**, 674-685.

Conway, J.W. and D.S. Zrnic, 1993: A study of production of hail growth using dual-Doppler and multiparameter radars. *Mon. Wea. Rev.*, **121**, 2511-2528.

Darkow, G.L. and D.W. McCann, 1977: Relative environmental winds for 121 tornado bearing storms. Preprints, *10th Conf. Severe Local Storms*, Omaha, NE, Amer. Meteor. Soc., 413-417.

Davies-Jones, R., 1984: Streamwise vorticity: The origin of updraft rotation in supercell thunderstorms. *J. Atmos. Sci.*, **41**, 2991-3006.

Dowell, D.C., C.R. Alexander, J.M. Wurman, and L.J. Wicker, 2005: Centrifuging of hydrometeors and debris in tornadoes: Radar reflectivity patterns and wind-measurement errors. *Mon. Wea. Rev.*, **133**, 1501-1524.

Droegemeier, K.K., S.M. Lazarus, and R.P. Davies-Jones, 1993: The influence of helicity on numerically simulated convective storms. *Mon. Wea. Rev.*, **121**, 2005-2029.

Fawbush, E.J. and R.C. Miller, 1954: The types of airmasses in which North American tornadoes form. *Bull. Amer. Meteor. Soc.*, **35,** 154-165.

Gunn, R. and G.D. Kinzer, 1949: The terminal velocity of fall for water droplets in stagnant air. *J. Meteor.*, **6**, 243-248.

Gunn, K.L.S. and J.S. Marshall, 1955: The effect of wind shear on falling precipitation. *J. Meteor.*, **12**, 339-349.

Kumjian, M.R. and A.V. Ryzhkov, 2007: Polarimetric characteristics of tornadic and nontornadic supercell thunderstorms. Extended Abstracts, *33rd Conf. Radar Meteorology*, Amer. Meteor. Soc., Cairns, Australia, P10.1.

Kumjian, M.R. and A.V. Ryzhkov, 2008: Polarimetric signatures in supercell thunderstorms. Submitted to *J. Appl. Meteor. Climat.*, 14 Sept. 2007. Submitted.

Maddox, R.A., 1976: An evaluation of tornado proximity wind and stability data. *Mon. Wea. Rev.*, **104**, 133-142.

Markowski, P.M., J.M. Straka, E.N. Rasmussen, and D.O. Blanchard, 1998: Variability of storm-relative helicity during VORTEX. *Mon. Wea. Rev.*, **126**, 2959-2971.

Pruppacher, H.R. and R.L. Pitter, 1971: A semi-empirical determination of the shape of cloud and raindrops. *J. Atmos. Sci.*, **28**, 86-94.

Ryzhkov, A.V., T.J. Schuur, D.W. Burgess, and D.S. Zrnic, 2005: Polarimetric tornado detection. *J. Appl. Meteor.*, **44**, 557-570.

Seliga, T.A. and V.N. Bringi, 1976: Potential use of radar differential reflectivity measurements at orthogonal polarizations for measuring precipitation. *J. Appl. Meteor.*, **15**, 69-76.

Ulbrich, C.W., 1983: Natural variations in the analytical form of the raindrop size distribution. *J. Climate Appl. Meteor.*, **22**, 1764-1775.

Wurman, J. and S. Gill, 2000: Finescale radar observations of the Dimmit, Texas (2 June 1995) tornado. *Mon. Wea. Rev.*, **128**, 2135-2164.

Wurman, J., J.M. Straka, and E.N. Rasmussen, 1996: Fine-scale Doppler radar observations of tornadoes. *Science*, **272**, 1774-1777.